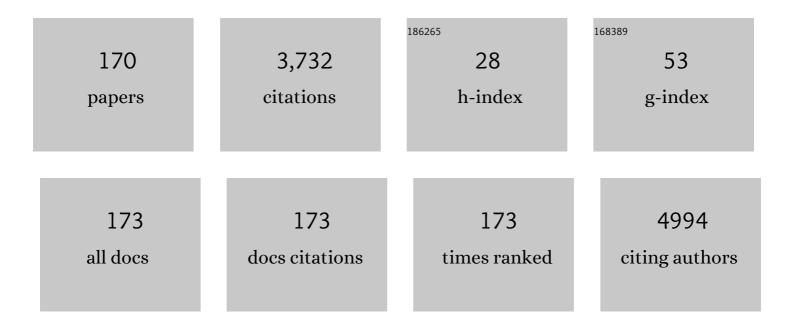
List of Publications by Year in descending order

Source: https://exaly.com/author-pdf/5040369/publications.pdf Version: 2024-02-01



Ιλμβέρτο Πίιδ2

#	Article	IF	CITATIONS
1	Stratigraphic analysis of intercalated graphite electrodes in aqueous inorganic acid solutions. Nano Research, 2022, 15, 1120-1127.	10.4	7
2	Reversible metamorphosis from Fe <sub>3</sub> O <sub>4</sub> to FeO of epitaxial iron oxide films grown on the Fe-p(1 × 1)O surface. RSC Advances, 2021, 11, 11513-11518.	3.6	2
3	Phonon-Mediated Interlayer Charge Separation and Recombination in a MoSe <sub>2</sub> /WSe <sub>2</sub> Heterostructure. Nano Letters, 2021, 21, 2165-2173.	9.1	46
4	An In-Depth Assessment of the Electronic and Magnetic Properties of a Highly Ordered Hybrid Interface: The Case of Nickel Tetra-Phenyl-Porphyrins on Fe(001)–p(1 × 1)O. Micromachines, 2021, 12, 191.	2.9	7
5	Outâ€Ofâ€Plane Metal Coordination for a True Solventâ€Free Building with Molecular Bricks: Dodging the Surface Ligand Effect for Onâ€Surface Vacuum Selfâ€Assembly. Advanced Functional Materials, 2021, 31, 2011008.	14.9	8
6	Frequency Tripling via Sum-Frequency Generation at the Nanoscale. ACS Photonics, 2021, 8, 1175-1182.	6.6	19
7	Mapping the evolution of Bi/Ge(111) empty states: From the wetting layer to pseudo-cubic islands. Journal of Applied Physics, 2021, 129, 155310.	2.5	2
8	Optical tuning of dielectric nanoantennas for thermo-optically reconfigurable nonlinear metasurfaces. Optics Letters, 2021, 46, 2453.	3.3	40
9	Epitaxial Growth: Outâ€Ofâ€Plane Metal Coordination for a True Solventâ€Free Building with Molecular Bricks: Dodging the Surface Ligand Effect for Onâ€Surface Vacuum Selfâ€Assembly (Adv. Funct. Mater.) Tj ETQq1	<b>1409</b> 7843	51 <b>⊈</b> rgBT /O√
10	Statistical Characterization of Heterogeneous Dissolution Rates of Calcite from In situ and Real-Time AFM Imaging. Transport in Porous Media, 2021, 140, 291-312.	2.6	6
11	Driving Organic Nanocrystals Dissolution Through Electrochemistry. ChemistryOpen, 2021, 10, 748-755.	1.9	2
12	Electrochemical scanning probe analysis used as a benchmark for carbon forms quality test. Journal of Physics Condensed Matter, 2021, 33, 115002.	1.8	2
13	Compared EC-AFM Analysis of Laser-Induced Graphene and Graphite Electrodes in Sulfuric Acid Electrolyte. Molecules, 2021, 26, 7333.	3.8	0
14	Observation of a Metastable Honeycomb Arrangement of C <sub>60</sub> on Ni(111) with (7 × 7) Periodicity: Tailoring an Interface for Organic Spintronics. ACS Applied Nano Materials, 2021, 4, 12993-13000.	5.0	2
15	Cobalt atoms drive the anchoring of Co-TPP molecules to the oxygen-passivated Fe(0â€ <sup>-</sup> 0â€ <sup>-</sup> 1) surface. Applied Surface Science, 2020, 505, 144213.	6.1	21
16	Disclosing the Graphite Surface Chemistry in Acid Solutions for Anion Intercalation. ACS Applied Nano Materials, 2020, 3, 691-698.	5.0	20
17	Customised porphyrin coating films for graphite electrode protection: An investigation on the role of peripheral groups by coupled AFM and cyclic voltammetry techniques. Applied Surface Science, 2020, 507, 145055.	6.1	1
18	Evidence of graphite blister evolution during the anion de-intercalation process in the cathodic regime. Applied Surface Science, 2020, 504, 144440.	6.1	11

#	Article	IF	CITATIONS
19	Electronic structure and magnetic behavior of ultra-thin Fe films grown on W(110) with a Co buffer layer. Journal of Electron Spectroscopy and Related Phenomena, 2020, 243, 146977.	1.7	0
20	Interaction of ultra-thin CoTPP films on Fe(001) with oxygen: Interplay between chemistry, order, and magnetism. Journal of Applied Physics, 2020, 128, .	2.5	7
21	Plasmonic Superchiral Lattice Resonances in the Mid-Infrared. ACS Photonics, 2020, 7, 2676-2681.	6.6	26
22	Ordered Porphyrin Arrays on Fe(001): An Enabling Technology for Future Spintronics. Proceedings (mdpi), 2020, 56, 25.	0.2	0
23	Anion intercalated graphite: a combined electrochemical and tribological investigation by in situ AFM. Journal of Microscopy, 2020, 280, 222-228.	1.8	3
24	Persistence of the Co-tetra-phenyl-porphyrin HOMO-LUMO features when a single organic layer is grown onto Cu(1Â1Â0)-(2Â×Â1)O. Applied Surface Science, 2020, 514, 145891.	6.1	6
25	3-dimensional nucleation of Fe oxide induced by a graphene buffer layer. Journal of Chemical Physics, 2020, 152, 054706.	3.0	3
26	In situ atomic force microscopy: the case study of graphite immersed in aqueous NaOH electrolyte. European Physical Journal Plus, 2020, 135, 1.	2.6	1
27	Porphycene Films Grown on Highly Oriented Pyrolytic Graphite: Unveiling Structure–Property Relationship through Combined Reflectance Anisotropy Spectroscopy and Atomic Force Microscopy Investigations. Proceedings (mdpi), 2020, 56, 44.	0.2	1
28	Reactive Dissolution of Organic Nanocrystals at Controlled pH. ChemNanoMat, 2020, 6, 567-575.	2.8	4
29	Empty electron states in cobalt-intercalated graphene. Journal of Chemical Physics, 2020, 153, 214703.	3.0	4
30	Superchiral Surface Waves for All-Optical Enantiomer Separation. Journal of Physical Chemistry C, 2019, 123, 28336-28342.	3.1	11
31	Evidence of Cascaded Third-Harmonic Generation in Noncentrosymmetric Gold Nanoantennas. Nano Letters, 2019, 19, 7013-7020.	9.1	23
32	Room temperature magnetism of ordered porphyrin layers on Fe. Applied Physics Letters, 2019, 115, .	3.3	12
33	Effects of the introduction of a chromium oxide monolayer at the C60/Fe(001) interface. Journal of Applied Physics, 2019, 125, 142907.	2.5	3
34	Graphene as an Ideal Buffer Layer for the Growth of High-Quality Ultrathin Cr <sub>2</sub> O <sub>3</sub> Layers on Ni(111). ACS Nano, 2019, 13, 4361-4367.	14.6	15
35	Temperature Effects on the HOPG Intercalation Process. Condensed Matter, 2019, 4, 23.	1.8	4
36	Incipient Anion Intercalation of Highly Oriented Pyrolytic Graphite Close to the Oxygen Evolution Potential: A Combined X-ray Photoemission and Raman Spectroscopy Study. Journal of Physical Chemistry C, 2019, 123, 1790-1797.	3.1	18

#	Article	IF	CITATIONS
37	The effect of cyclic voltammetry speed on anion intercalation in HOPG. Surface Science, 2019, 681, 111-115.	1.9	8
38	Magnetic properties of the CoO/Fe(001) system with a bottom-up engineered interface. Journal of Magnetism and Magnetic Materials, 2019, 475, 54-59.	2.3	3
39	CVD Graphene/Ni Interface Evolution in Sulfuric Electrolyte. Langmuir, 2018, 34, 3413-3419.	3.5	9
40	Morphological changes of porphine films on graphite by perchloric and phosphoric electrolytes. Applied Surface Science, 2018, 442, 501-506.	6.1	13
41	Contact potential and scanning Kelvin force microscopy measurements on sulphate-anion intercalated graphite. Electrochimica Acta, 2018, 267, 20-23.	5.2	4
42	Chemical characterization of fluorinated/hydrogenated mixed monolayers grafted on gold nanoparticles. Journal of Fluorine Chemistry, 2018, 206, 99-107.	1.7	5
43	Blister evolution time invariance at very low electrolyte pH: H2SO4/graphite system investigated by electrochemical atomic force microscopy. Electrochimica Acta, 2018, 276, 352-361.	5.2	14
44	Plasmon-Enhanced Second Harmonic Sensing. Journal of Physical Chemistry C, 2018, 122, 11475-11481.	3.1	15
45	Local structure and morphological evolution of ZnTPP molecules grown on Fe(001)-p(1 × 1)O studied l STM and NEXAFS. Applied Surface Science, 2018, 435, 841-847.	by 6.1	16
46	Spinâ€Resolved PES and IPES Investigation of the Graphene/Ni(111) Interface. Physica Status Solidi (B): Basic Research, 2018, 255, 1700415.	1.5	5
47	Metal–dielectric hybrid nanoantennas for efficient frequency conversion at the anapole mode. Beilstein Journal of Nanotechnology, 2018, 9, 2306-2314.	2.8	47
48	Surfaceâ€enhanced chiroptical spectroscopy with superchiral surface waves. Chirality, 2018, 30, 883-889.	2.6	19
49	Template Assisted Nucleation of Cobalt and Gold Nano-clusters on an Ultrathin Iron Oxide Film. Topics in Catalysis, 2018, 61, 1283-1289.	2.8	0
50	Drastic Improvement of Air Stability in an n-Type Doped Naphthalene-Diimide Polymer by Thionation. ACS Applied Energy Materials, 2018, 1, 4626-4634.	5.1	39
51	Vacuum-Deposited Porphyrin Protective Films on Graphite: Electrochemical Atomic Force Microscopy Investigation during Anion Intercalation. ACS Applied Materials & Interfaces, 2017, 9, 4100-4105.	8.0	19
52	Thermoelectric Properties of Highly Conductive Poly(3,4-ethylenedioxythiophene) Polystyrene Sulfonate Printed Thin Films. ACS Applied Materials & Interfaces, 2017, 9, 18151-18160.	8.0	27
53	Temporal analysis of blister evolution during anion intercalation in graphite. Physical Chemistry Chemical Physics, 2017, 19, 13855-13859.	2.8	26
54	Microscopic Analysis of the Different Perchlorate Anions Intercalation Stages of Graphite. Journal of Physical Chemistry C, 2017, 121, 14246-14253.	3.1	23

#	Article	IF	CITATIONS
55	Intercalation from the Depths: Growth of a Metastable Chromium Carbide between Epitaxial Graphene and Ni(111) by Carbon Segregation from the Bulk. Journal of Physical Chemistry C, 2017, 121, 16803-16809.	3.1	9
56	Enhanced Magnetic Hybridization of a Spinterface through Insertion of a Two-Dimensional Magnetic Oxide Layer. Nano Letters, 2017, 17, 7440-7446.	9.1	17
57	Anomalous local lattice disorder and distortion in A2Mo2O7 pyrochlores. Journal of Alloys and Compounds, 2017, 723, 327-332.	5.5	2
58	Chiral surface waves for enhanced circular dichroism. Physical Review B, 2017, 95, .	3.2	42
59	Plasmon-Enhanced Second Harmonic Generation: from Individual Antennas to Extended Arrays. Plasmonics, 2017, 12, 1595-1600.	3.4	8
60	Polarization properties of second-harmonic generation in AlGaAs optical nanoantennas. Optics Letters, 2017, 42, 559.	3.3	57
61	Polarization-resolved second harmonic generation measurements in AlGaAs monolithic nanoantennas. , 2017, , .		0
62	Evolution of the graphite surface in phosphoric acid: an AFM and Raman study. Beilstein Journal of Nanotechnology, 2016, 7, 1878-1884.	2.8	22
63	Atomic Scale Insights into the Early Stages of Metal Oxidation: A Scanning Tunneling Microscopy and Spectroscopy Study of Cobalt Oxidation. Journal of Physical Chemistry C, 2016, 120, 5233-5241.	3.1	14
64	Structure and electronic properties of Zn-tetra-phenyl-porphyrin single- and multi-layers films grown on Fe(001)-p(1 × 1)O. Applied Surface Science, 2016, 390, 856-862.	6.1	19
65	Electronic and magnetic structure of ultra-thin Ni films grown on W(110). Journal of Magnetism and Magnetic Materials, 2016, 420, 356-362.	2.3	5
66	Controlling the Electronic and Structural Coupling of C <sub>60</sub> Nano Films on Fe(001) through Oxygen Adsorption at the Interface. ACS Applied Materials & Interfaces, 2016, 8, 26418-26424.	8.0	23
67	Spin polarized surface resonance bands in single layer Bi on Ge(1 1 1). Journal of Physics Condensed Matter, 2016, 28, 195001.	1.8	10
68	Observation of Mixed Valence Ru Components in Zn Doped Y <sub>2</sub> Ru <sub>2</sub> O <sub>7</sub> Pyrochlores. Journal of Physical Chemistry C, 2016, 120, 11763-11768.	3.1	23
69	Self-organized nano-structuring of CoO islands on Fe(001). Applied Surface Science, 2016, 362, 374-379.	6.1	12
70	Reactive metal–oxide interfaces: A microscopic view. Surface Science Reports, 2016, 71, 32-76.	7.2	80
71	Disclosing the Early Stages of Electrochemical Anion Intercalation in Graphite by a Combined Atomic Force Microscopy/Scanning Tunneling Microscopy Approach. Journal of Physical Chemistry C, 2016, 120, 6088-6093.	3.1	43
72	Quasistatic limit for plasmon-enhanced optical chirality. Physical Review B, 2015, 91, .	3.2	17

#	Article	IF	CITATIONS
73	Optical and morphological properties of ultra-thin H <sub>2</sub> TPP, H <sub>4</sub> TPP and ZnTPP films. Physica Status Solidi (B): Basic Research, 2015, 252, 100-104.	1.5	7
74	Evidence of a correlation between magnetic and structural transitions in Y2â^'xZnxRu2O7 pyrochlore compounds. RSC Advances, 2015, 5, 100809-100815.	3.6	8
75	2D-3D Phase Transition in Ultra-thin H2TPP Films Induced by Deposition of Iron Atoms. Materials Today: Proceedings, 2015, 2, 4239-4246.	1.8	1
76	Fully-printed, all-polymer, bendable and highly transparent complementary logic circuits. Organic Electronics, 2015, 20, 132-141.	2.6	68
77	Mode matching in multiresonant plasmonic nanoantennas for enhanced second harmonic generation. Nature Nanotechnology, 2015, 10, 412-417.	31.5	421
78	Elucidating the Impact of Molecular Packing and Device Architecture on the Performance of Nanostructured Perylene Diimide Solar Cells. ACS Applied Materials & Interfaces, 2015, 7, 8687-8698.	8.0	26
79	Oxygen-induced immediate onset of the antiferromagnetic stacking in thin Cr films on Fe(001). Applied Physics Letters, 2015, 106, 162408.	3.3	9
80	Stability of Organic Cations in Solution-Processed CH <sub>3</sub> NH <sub>3</sub> Pbl <sub>3</sub> Perovskites: Formation of Modified Surface Layers. Journal of Physical Chemistry C, 2015, 119, 21329-21335.	3.1	79
81	Emission Engineering in Germanium Nanoresonators. ACS Photonics, 2015, 2, 53-59.	6.6	27
82	Electron spectroscopy investigation of the oxidation of ultra-thin films of Ni and Cr on Fe(0 0 1). Journal of Physics Condensed Matter, 2014, 26, 445001.	1.8	14
83	Organic Electronics: Stable Alignment of Tautomers at Room Temperature in Porphyrin 2D Layers (Adv.) Tj ETQq	1 1,0.7843	314 rgBT /Cve
84	Unconventional postâ€deposition chemical treatment on ultraâ€ŧhin H <sub>2</sub> TPP film grown on graphite. Crystal Research and Technology, 2014, 49, 581-586.	1.3	9
85	Epitaxial growth of thin TiO <sub>2</sub> films on the Au covered Fe(100) surface. Crystal Research and Technology, 2014, 49, 587-593.	1.3	1
86	Stable Alignment of Tautomers at Room Temperature in Porphyrin 2D Layers. Advanced Functional Materials, 2014, 24, 958-963.	14.9	51
87	Photoemission study of the Poly(3-hexylthiophene)/TiO2 interface and the role of 4-Mercaptopyridine. Thin Solid Films, 2014, 560, 39-43.	1.8	6
88	Oxidation effects on ultrathin Ni and Cr films grown on Fe(001): A combined scanning tunneling microscopy and Auger electron spectroscopy study. Surface Science, 2014, 621, 55-63.	1.9	17
89	Controlling drop-casting deposition of 2D Pt-octaethyl porphyrin layers on graphite. Synthetic Metals, 2014, 195, 201-207.	3.9	12
90	Probing Two-Dimensional vs Three-Dimensional Molecular Aggregation in Metal-Free Tetraphenylporphyrin Thin Films by Optical Anisotropy. Journal of Physical Chemistry C, 2014, 118, 15649-15655.	3.1	23

#	Article	IF	CITATIONS
91	X-ray photoemission spectroscopy investigation of the early stages of the oxygen aided Cr growth on Fe(001). Applied Surface Science, 2013, 267, 141-145.	6.1	8
92	Laser-Induced Magnetic Nanostructures with Tunable Topological Properties. Physical Review Letters, 2013, 110, 177205.	7.8	256
93	X-ray Photoemission Spectroscopy Investigation of the Interaction between 4-Mercaptopyridine and the Anatase TiO2 Surface. Langmuir, 2013, 29, 8302-8310.	3.5	18
94	Growth and Interface Reactivity of Titanium Oxide Thin Films on Fe(001). Journal of Physical Chemistry C, 2013, 117, 9229-9236.	3.1	16
95	Magnetic properties of monolayer range chromium oxides on Fe(001). Journal of Applied Physics, 2013, 114, .	2.5	9
96	Dynamics of Four-Photon Photoluminescence in Gold Nanoantennas. Nano Letters, 2012, 12, 2941-2947.	9.1	81
97	Circular Dichroism Probed by Two-Photon Fluorescence Microscopy in Enantiopure Chiral Polyfluorene Thin Films. Journal of the American Chemical Society, 2012, 134, 5832-5835.	13.7	28
98	Growth of stoichiometric TiO2 thin films on Au(100) substrates by molecular beam epitaxy. Thin Solid Films, 2012, 520, 3922-3926.	1.8	13
99	Thermal Instability of Thin Ni/Fe(001) Films. Nanoscience and Nanotechnology Letters, 2012, 4, 1092-1095.	0.4	6
100	Spontaneous Formation of Left- and Right-Handed Cholesterically Ordered Domains in an Enantiopure Chiral Polyfluorene Film. Journal of Physical Chemistry Letters, 2011, 2, 1359-1362.	4.6	15
101	Effects of temperature on the oxygen aided Cr growth on Fe(001). Surface Science, 2011, 605, 2092-2096.	1.9	21
102	Scanning tunneling microscopy investigation of CoO/Fe(001) and Fe/CoO/Fe(001) layered structures. Surface Science, 2011, 605, 95-100.	1.9	11
103	Oxygen-induced effects on the morphology of the Fe(001) surface in out-of-equilibrium conditions. Physical Review B, 2011, 83, .	3.2	38
104	The fundamentals of flame treatment for the surface activation of polyolefin polymers – A review. Polymer, 2010, 51, 3591-3605.	3.8	107
105	Macroscopic movement of azo polymer chains by nearâ€field probes: Dependence on the illumination conditions. Physica Status Solidi (B): Basic Research, 2010, 247, 2067-2070.	1.5	2
106	Recent developments in linear and nonlinear nearâ€field microscopy on single plasmonic nanoparticles. Physica Status Solidi (B): Basic Research, 2010, 247, 2040-2046.	1.5	8
107	Experimental Observation of a Photon Bouncing Ball. Physical Review Letters, 2009, 102, 180402.	7.8	44
108	Magnetic properties of interfaces and multilayers based on thin antiferromagnetic oxide films. Surface Science Reports, 2009, 64, 139-167.	7.2	74

#	Article	IF	CITATIONS
109	All-optical subdiffraction multilevel data encoding onto azo-polymeric thin films. Optics Letters, 2009, 34, 761.	3.3	22
110	Near-field circular polarization probed by chiral polyfluorene. Optics Letters, 2009, 34, 3571.	3.3	17
111	Cross Resonant Optical Antenna. Physical Review Letters, 2009, 102, 256801.	7.8	179
112	Epitaxial growth and characterization of CoO/Fe(001) thin film layered structures. Thin Solid Films, 2008, 516, 7519-7524.	1.8	29
113	Evidence of photoinduced charge transfer in C60/GaAs(100) bilayers by pump–probe measurements. Chemical Physics Letters, 2008, 466, 65-67.	2.6	7
114	Mapping local field enhancements at nanostructured metal surfaces by second-harmonic generation induced in the near field. Journal of Microscopy, 2008, 229, 233-239.	1.8	10
115	Experimental demonstration of the optical Zeno effect by scanning tunneling optical microscopy. Optics Express, 2008, 16, 3762.	3.4	62
116	Combined spectroscopic characterization of electron transfer at hybrid CuPcF16/GaAs semiconductor interfaces. Nanotechnology, 2008, 19, 424010.	2.6	5
117	Bulk Cr tips for scanning tunneling microscopy and spin-polarized scanning tunneling microscopy. Applied Physics Letters, 2007, 91, .	3.3	39
118	Discrete diffraction in waveguide arrays: A quantitative analysis by tunneling optical microscopy. Applied Physics Letters, 2007, 90, .	3.3	14
119	High-resolution imaging of local oxidation in polyfluorene thin films by nonlinear near-field microscopy. Applied Physics Letters, 2007, 91, 191118.	3.3	13
120	Space charge effects on the active region of a planar organic photodetector. Journal of Applied Physics, 2007, 101, 114504.	2.5	32
121	Early stages of interface formation of C60 on GaAs(100). Surface Science, 2007, 601, 4078-4081.	1.9	9
122	Magnetic Nanostructures: In-Situ Assembly and Exploration of Low-Dimensional Systems by Spin-Polarized Low-Energy Electron Microscopy. Microscopy and Microanalysis, 2006, 12, 964-965.	0.4	0
123	Direct observation of magnetic instabilities in NiO thin films epitaxially grown on Fe(001). Surface Science, 2006, 600, 4160-4165.	1.9	12
124	Nano-sized magnetic instabilities in Fe/NiO/Fe(001) epitaxial thin films. Thin Solid Films, 2006, 515, 712-715.	1.8	5
125	Onset of ferromagnetism in ultrathin Fe films on semiconductors. Solid State Communications, 2005, 135, 158-161.	1.9	8
126	Near-field vs. far-field polarization properties of hollow pyramid SNOM tips. Physica Status Solidi C: Current Topics in Solid State Physics, 2005, 2, 4078-4082.	0.8	3

#	Article	IF	CITATIONS
127	Spin-Polarized Tunneling Spectroscopy in Tunnel Junctions with Half-Metallic Electrodes. Physical Review Letters, 2005, 95, 137203.	7.8	82
128	Unexpected polarization behavior at the aperture of hollow-pyramid near-field probes. Applied Physics Letters, 2005, 87, 223112.	3.3	46
129	Looking 100 AÌŠ deep into spatially inhomogeneous dilute systems with hard x-ray photoemission. Applied Physics Letters, 2004, 85, 4532.	3.3	71
130	Spin and energy analysis of electron beams: Coupling a polarimeter based on exchange scattering to a hemispherical analyzer. Review of Scientific Instruments, 2002, 73, 3867-3871.	1.3	23
131	Versatile apparatus for investigating ultrathin magnetic films. Journal of Electron Spectroscopy and Related Phenomena, 2002, 122, 221-229.	1.7	5
132	Epitaxial thin NiO films grown on Fe(001) and the effect of temperature. Surface Science, 2002, 518, 234-242.	1.9	28
133	Evolution of the magnetic and electronic properties of ultrathin Cr(001) films. Solid State Communications, 2000, 116, 283-286.	1.9	10
134	Multiatomic resonant photoemission spectroscopy on CuO and NiO: Observation of antiresonant behavior. Physical Review B, 2000, 62, R16215-R16218.	3.2	11
135	Electronic and magnetic properties of the Co/Fe(001) interface and the role of oxygen. Physical Review B, 2000, 61, 15294-15301.	3.2	22
136	Structural and magnetic properties of the Ce/Fe(001) interface: a spin resolved inverse photoemission study. Surface Science, 1999, 440, 301-306.	1.9	0
137	Surface effects in the spectroscopy of mixed-valent Ce compounds. Surface Science Reports, 1998, 32, 235-289.	7.2	24
138	Input electron optics for Mott detectors used in secondary electron magnetometry. Journal of Electron Spectroscopy and Related Phenomena, 1998, 95, 255-260.	1.7	1
139	Electronic structure of CeSe probed by resonant photoemission spectroscopy: A test case for the single-impurity Anderson Hamiltonian. Physical Review B, 1998, 57, 12030-12035.	3.2	6
140	Surface and bulk4f-photoemission spectra ofCeIn3andCeSn3. Physical Review B, 1997, 56, 1620-1624.	3.2	32
141	The Ce4fsurface shift: A test for the Anderson-impurity Hamiltonian. Physical Review B, 1996, 54, R17363-R17366.	3.2	16
142	Hybridization effects in unoccupied 4fstates of Ce compounds. Physical Review B, 1996, 53, 7030-7034.	3.2	12
143	A Cooper minimum photoemission study of the alloy. Journal of Physics Condensed Matter, 1996, 8, 1413-1419.	1.8	4
144	The localisation of 3d hole states in Fe and FeAl studied by Auger vacancy satellite spectroscopy. Journal of Electron Spectroscopy and Related Phenomena, 1995, 72, 205-209.	1.7	24

LAMBERTO DUÃ<sup>2</sup>

#	Article	IF	CITATIONS
145	Copper L3-M4,5M4,5 Auger and Auger satellite structures in polycrystalline Cu50Pd50 alloy. Journal of Electron Spectroscopy and Related Phenomena, 1995, 72, 217-221.	1.7	2
146	Sensitivity of the valence states upon rare earth substitution in intermetallic compounds. Journal of Electron Spectroscopy and Related Phenomena, 1995, 76, 517-522.	1.7	3
147	Bulk electronic structure of Ce compounds studied by x-ray photoemission and x-ray absorption spectroscopies. Physical Review B, 1995, 52, 16503-16507.	3.2	13
148	Effects of Ce-Lu substitution on thedvalence states of Laves phases. Physical Review B, 1995, 51, 4751-4754.	3.2	10
149	Polarized Unoccupied States of Oxygen on Fe(100). Europhysics Letters, 1995, 32, 687-692.	2.0	12
150	Effects of Ce vs. Lu substitution on the electronic structure of rare earth-transition metal compounds. Journal of Alloys and Compounds, 1995, 225, 432-435.	5.5	1
151	A high-efficiency photon detector for parallel acquisition of UV inverse photoemission spectroscopy. Measurement Science and Technology, 1994, 5, 1015-1017.	2.6	6
152	Charge-Transfer Satellites in K <i>L</i> <sub>23</sub> XAS Data for K/Si(111)-(2 × 1): Evidence for Strong Ionic Bonds. Europhysics Letters, 1994, 26, 85-90.	2.0	11
153	UV-spectroscopy study of theCe7Rh3empty and filled valence states. Physical Review B, 1994, 50, 9561-9564.	3.2	9
154	Can We Describe the Spectral Function of CeRh3by a Band Picture?. Physical Review Letters, 1994, 73, 2005-2005.	7.8	25
155	Empty and filled valence-electron states of Lu–transition-metal compounds: An uv spectroscopy study. Physical Review B, 1994, 49, 10159-10165.	3.2	11
156	A novel soft X-ray source (hν = 151.6 eV) for core level and valence band photoemission spectroscopy with high surface sensitivity. Journal of Electron Spectroscopy and Related Phenomena, 1993, 62, 309-316.	1.7	1
157	Interaction of oxygen with polycrystalline cobalt studied by inverse-photoemission spectroscopy. Physical Review B, 1993, 47, 15848-15851.	3.2	11
158	Strong evolution of thep-projected empty density of states in Pd-Al alloys: AnM4,5x-ray-absorption-spectroscopy investigation. Physical Review B, 1993, 47, 6937-6941.	3.2	5
159	Energy dependence of 4fand 5dcross sections for rare-earth metals. Physical Review B, 1993, 48, 10728-10732.	3.2	26
160	Solid-state effects on Ag in dilute alloys revealed by Cooper-minimum photoemission. Physical Review B, 1992, 46, 3747-3753.	3.2	19
161	P-derived valence states at the reactive GaP(110)/Yb interface via PL2,3VVAuger line-shape spectroscopy. Physical Review B, 1992, 45, 6255-6258.	3.2	3
162	Synchrotron-radiation investigation of the chemical dependence of the vacancy-satellite structure of the NiL3VVspectra in Ni silicides. Physical Review B, 1992, 46, 15652-15659.	3.2	5

#	Article	IF	CITATIONS
163	Anion-specific surface valence-band states in heteropolar semiconductors: The case of GaP(110) and InP(110). Physical Review B, 1992, 46, 13607-13610.	3.2	1
164	The virtual bound states of Fe in AuFe studied by photoemission. Journal of Physics Condensed Matter, 1991, 3, 989-995.	1.8	6
165	Off-Site Contributions to Electron Correlation; An Extension to the Hubbard Model Studied by Auger Spectroscopy. Europhysics Letters, 1991, 16, 743-749.	2.0	20
166	N6,7O4,5O4,5Auger spectrum of metallic Au. Physical Review B, 1991, 43, 9550-9557.	3.2	19
167	Yb interface growth on GaP(110): an electron spectroscopy investigation. Vacuum, 1990, 41, 1065-1067.	3.5	3
168	Simplification of the N6.7O4.5O4.5Auger spectrum of Au. Journal of Physics Condensed Matter, 1990, 2, 195-200.	1.8	11
169	Strong chemical reactivity at the early stages of Yb overgrowth on GaP(110): A synchrotron-radiation study. Physical Review B, 1990, 42, 3478-3484.	3.2	18
170	A Stable Porphyrin Functionalized Graphite Electrode Used at the Oxygen Evolution Reaction Potential. Electroanalysis, 0, , .	2.9	0